MDPI

Article

Experimental Study of CO$_2$-ECBM by Injection Liquid CO$_2$

Mingyang Liu [1,2,*] , Hu Wen [1,2], Shixing Fan [1,2], Zhenping Wang [1,2], Jinbiao Fei [1,2], Gaoming Wei [1,2], Xiaojiao Cheng [1,2] and Hu Wang [1,2]

[1] College of Safety Science and Engineering, Xi'an University of Science and Technology, Xi'an 710054, China; wenh@xust.edu.cn (H.W.); fanxing@xust.edu.cn (S.F.); wzp147258369@sina.com (Z.W.); feijinb@xust.edu.cn (J.F.); 18120089022@stu.xust.edu.cn (G.W.); 201512713@stu.xust.edu.cn (X.C.); 19120089013@stu.xust.edu.cn (H.W.)

[2] Shaanxi Key Laboratory of Prevention and Control of Coal Fire, Xi'an 710054, China

* Correspondence: 17120089012@stu.xust.edu.cn

Abstract: Coal mine gas disasters have severely restricted production safety. Improving gas extraction efficiency can effectively reduce disasters. Scholars have confirmed that CO$_2$ successfully displaces coal seam CH$_4$. This study conducted displacement and in situ experiments and compared gas drainage under different injection pressures. The displacement experiments indicated that CH$_4$ production rates increased under increased pressures while the displacement ratios decreased. The pressure had a positive effect on sweep efficiency. The in situ experiment showed that CH$_4$ and CO$_2$ concentration trends in the inspection hole remained consistent. Through observing the data of the original and inspection holes, the average gas drainage concentration during low- and medium-pressure injections increased by 0.61 times and 1.17 times, respectively. The low-pressure average gas drainage scalar was increased by 1.08 times. During the medium-pressure injection, the average gas drainage purity increased by 1.94 times. The diffusion ranges of CO$_2$ under low- and medium-pressure injections were 20–25 m and 25–30 m, respectively. The sweep efficiency of medium-pressure injection was 26% better than that of the low-pressure injection, with average pressures of 2.8 MPa and 1.4 MPa, respectively, for sweep efficiency. This study proposes an effective method for improving coal mine gas drainage efficiency.

Keywords: liquid CO$_2$; displacement; drainage effect; sweep efficiency

1. Introduction

Gas disasters are one of the most important factors affecting the safety of coal mining. Gas drainage is the most direct and effective method for controlling gas disasters and is also an effective way to obtain clean energy [1]. However, there are still some problems in coal mine gas extraction in low-permeability coal seams in China, such as a small influence range, difficult extraction, and fast attenuation [2,3]. Data statistics show that more than 95% of outburst and high-gas mines in China are in low-permeability coal seams, and the permeability is mostly 10^{-6}–10^{-7} μm^2 [4]. The gas extraction technology for low-permeability coal seams at home and abroad focus on improving coal seam permeability and increasing gas desorption [5–7].

Domestic and foreign scholars have developed a variety of coal seam permeability enhancements and gas drainage technologies and have carried out field tests in many mining areas to improve coalbed methane recovery. These include pore fracture reconstruction technologies such as hydraulic fracturing, explosive blasting, shock wave fracturing, L-CO$_2$ blasting, and L-CO$_2$ fracturing [8–14], and gas desorption technologies such as gas injection, heat injection, and acoustic waves [15–19].

However, these technologies have drawbacks. For instance, hydraulic fracturing and hydraulic cutting require large amounts of water. During the extraction process, the water block effect significantly affects methane extraction. Detonation wave fracturing

can result in the formation of a stress-concentrated area in the coalbed, thus increasing the possibility of accidents. Therefore, these technologies do not significantly improve the efficiency of coalbed methane recovery in coal seams. The gas phase displacement technology, which uses the competitive adsorption mechanism of adsorbed gas, increases the amount of gas desorption and improves the production of coalbed methane [20]. The study of gas displacement in coal seams is mainly concentrated on single or multiple gas injection experiments using CO_2 and N_2 gas, and the effect of gas displacement is evaluated by observing the replacement rate after gas injection [18]. The mechanism of gas phase displacement was revealed by studying the coal adsorption capacity to different gases and the competitive adsorption law of mixed gases [21,22].

In foreign countries, the first experimental study on coal gas displacement was conducted in a laboratory. CO_2 gas was injected into the coal core at a low pressure [23]. Gas injection was found to significantly improve the recovery rate of CH_4 through a comparison of the emission and natural desorption rates [24–26]. After injecting CO_2 into coal, the changes in the coal seam gas pressure and permeability were studied, and the key parameters in the process of methane replacement were obtained [27,28]. The injection of CO_2, N_2, and mixed gas for the enhanced coalbed methane recovery was also studied. The results revealed that the recovery efficiency of CH_4 by pure CO_2 was higher than the recovery efficiency by pure N_2 [29]. Mixed-gas injection reduces the efficiency of CH4 recovery. L-CO_2 is a cryogenic fluid with advantages such as a low viscosity, easy seepage diffusion, and high adsorption capacity. Injecting CO_2 into a coalbed at a constant low pressure improves the coalbed permeability under frost heaving and phase transformation forces generated by L-CO_2 [30–32].

Therefore, based on the low-viscosity permeability and displacement characteristics of L-CO_2, this study designs an engineering test of L-CO_2 displacing coal seam CH_4 technology [33,34]. Through the injection at different displacement pressures, the gas drainage concentration and purity after displacement were investigated, and the sweep efficiencies of different displacement pressures were compared and analyzed. This study provides a theoretical basis for L-CO_2 displacing coal seam CH_4 technology and new technical methods to improve gas drainage efficiency.

2. Theory and Experiment

2.1. Theoretical Analyses

According to the Langmuir adsorption theory, assuming that gas adsorption occurs on a monolayer solid surface, the proportion of adsorbent surface occupied θ is the coverage, and the ratio of the blank surface is $1 - \theta$ [35].

$$\theta = \frac{bP}{1 + bP} \tag{1}$$

where θ is the coverage, b is the adsorption coefficient, and P is the equilibrium pressure. Assuming that a certain amount of CH_4 has been adsorbed by coal, the adsorption law after CO_2 injection can be expressed by a thermodynamic equation.

$$\frac{dx}{dt} = k\theta_{CO_2}\theta_{CH_4} = \frac{kb_{CO_2}P_{CO_2}b_{CH_4}P_{CH_4}}{\left(1 + b_{CO_2}P_{CO_2} + b_{CH_4}P_{CH_4}\right)^2} \tag{2}$$

where dx/dt is the desorption rate and θ_{CO_2}, θ_{CH_4} are the coverage of CO_2 and CH_4. The coal adsorption capacity to CO_2 is stronger than that of CH_4, and it can be concluded that $b_{CH_4}P_{CH_4} \leq b_{CO_2}P_{CO_2} + 1$. The desorption rate can be simplified as follows:

$$\frac{dx}{dt} \approx \frac{kb_{CO_2}P_{CO_2}b_{CH_4}P_{CH_4}}{\left(1 + b_{CO_2}P_{CO_2}\right)^2} \tag{3}$$

The CH_4 partial pressure remains constant, and with the increase in CO_2 partial pressure, the replacement rate will have a maximum value. The partial pressure of CO_2 is constant when the partial pressure of CH_4 decreases gradually, and the replacement rate range decreases linearly [36].

When the CH_4 extraction was carried out by bed drilling, the permeability of the coal seam in the vertical direction was lower than that along the coal seam's horizontal direction. Therefore, the Darcy seepage flow along the bedding borehole by CO_2 injection can be expressed as follows [31]:

$$Q = A \frac{K}{\mu} \frac{\Delta P}{L_x} \tag{4}$$

where Q is the flow rate in m^3/s, A is the area of the cross-section in m^2, and μ is the viscosity of the fluid ($\mu Pa \cdot s$). K is the coefficient of proportionality, called permeability, in μm^2. $\Delta P / L_x$ is the pressure loss when a fluid flows across a distance L in a porous medium, MPa/m. However, in situ test results have revealed that the efficiency of CH_4 extraction is not heavily dependent on the radius and length of the borehole. In the process of enhancing coalbed methane by injecting CO_2 into the coal seam, the influence range of CO_2 was primarily affected by pressure.

When injecting liquid CO_2 into the coal seam, it was affected by three comprehensive effects: phase change pressurization, low-viscosity permeability, and displacement desorption. Under the freezing or heating phase change pressurization, the expansion and extension of original fractures and the generation of new fractures increase permeability. The seepage and diffusion of CO_2 into the coal and the competitive adsorption with CH_4 at the corresponding adsorption sites are generated under a pressure difference and concentration gradient. Finally, under the partial pressure and concentration difference of CO_2 injection, CH_4 gas on the adsorption site in the coal matrix was replaced and displaced, so that it migrated and diffused along the coal seam gas seepage channel to the gas drainage borehole, thereby improving the efficiency of coal seam gas drainage [37,38].

2.2. Experiment of Displacing Coal Seam CH_4 by CO_2

Since the main role in the whole process is the driven influence and displacement of CO_2. Compared with the whole displacement process, the L-CO_2 phase transition time (about 120 min) is shorter, and the influence range is limited. CO_2 plays a more important role. Additionally, L-CO_2 was easy to transport in the underground test and could be stored in large quantities in the CH_4 displacement experiment. Therefore, the gas phase displacement process is considered in a laboratory displacement experiment.

(1) Experimental preparation

The coal sample was taken from the #4 coal seam in the Mengcun coal mine of Binchang mining area in Shaanxi Province. A complete coal block of approximately 0.8 m $\times$ 0.8 m was taken from mining area, and 6 core samples of approximately 25 mm $\times$ 60 mm were chosen by the sampling drilling tool. The coal sample had a different microstructure than the pores and cracks of the coal seam. After the permeability test, three coal samples with similar permeabilities were selected. Therefore, the coal sample of the same coal block had little influence on the experimental results. The coal samples were placed into the gripper after drying, and the tightness of the gripper was checked before the experiment. CH_4 was injected into the coal samples by the pressure injection system to ensure that the coal samples fully absorbed CH_4, and then CO_2 was injected. After the pressure balanced out, the flow rate and gas composition of the output gas were monitored by adjusting the outlet pressure. The main parameters of the displacement experiments are listed in Table 1. The pressure and temperature corresponding to the critical point of CO_2 are 7.38 MPa and 31.04 °C. To ensure the gas phase state of CO_2 during injection, the experimental temperature was set at 30 °C and the injection pressure was controlled between 2.0 MPa and 7.0 MPa.

Table 1. The main parameters of displacement experiment.

Numbering	Size of Coal Sample (mm)	CH$_4$ Adsorption Pressure (MPa)	CH$_4$ Adsorption Time (h)	Confining Pressure (MPa)	CO$_2$ Injection Pressure (MPa)	Back Pressure (MPa)	Temperature (°C)
1#	25.1 × 60.0	1.0–2.0	16–24	8	2.0–3.0	1.0–1.5	30
2#	24.9 × 61.0	1.0–2.0	16–24	8	4.0–5.0	2.0–3.0	30
3#	25.0 × 59.0	1.0–2.0	16–24	8	6.0–7.0	4.0–5.0	30

(2) Experimental structure

The experimental system for displacing CH$_4$ from the coal seam by injecting CO$_2$ is composed of CH$_4$, a CO$_2$ injection system, a temperature control system, a core holder, a pressure control system, a data acquisition system, and a gas collection system. The experimental setup is shown in Figure 1. The CO$_2$ injection system was pressurized using a booster pump with a maximum pressure of 15 MPa. The temperature control unit used a constant-temperature control box to adjust the ambient temperature of the holder. The instantaneous flows and cumulative flows of CH$_4$ and CO$_2$ were measured using a mass flowmeter. The data acquisition system collected the flow and pressure information in the injection process, the confining pressure of the holder, the back pressure of the outlet, and the flow and concentration of the outlet mixed gas. The gas acquisition system measured the instantaneous flow and cumulative flow of the mixed gas using a flow meter, and the concentration of the mixed gas was analyzed by gas chromatography [39].
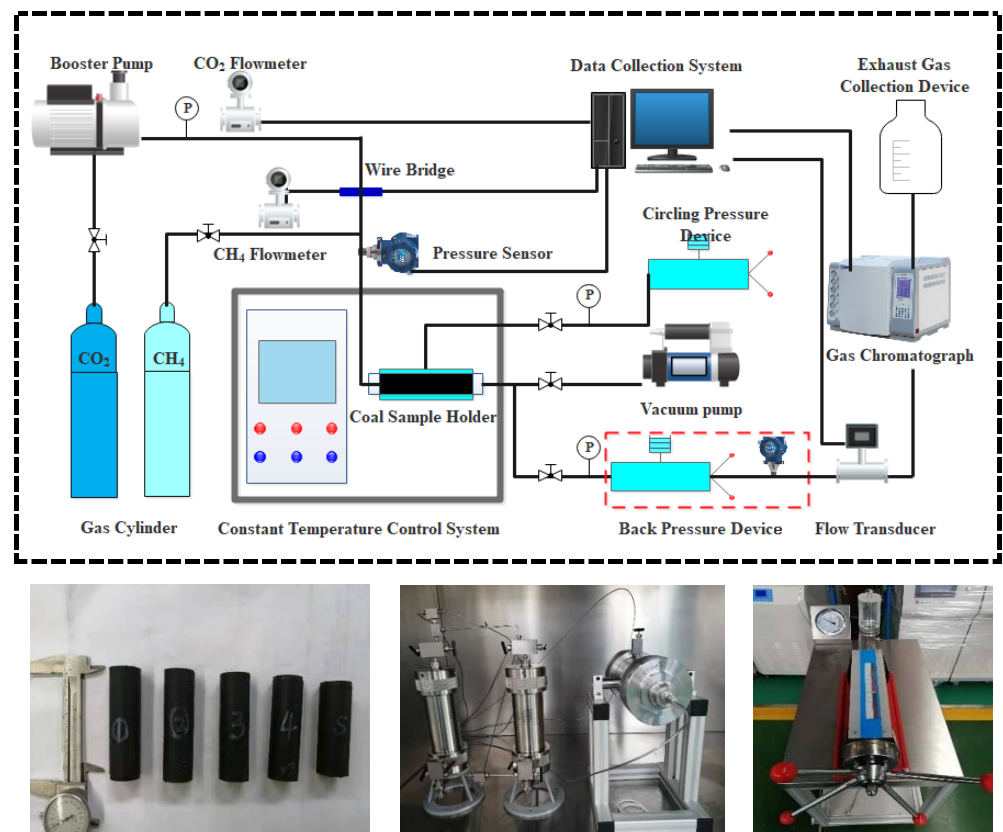
Figure 1. The experimental system diagram of CO$_2$ displacement coal seam CH$_4$.

(3) Experimental procedure

    1. Vacuuming: The inlet stop valve was closed, and the vacuum pump was connected to the sample holder at the outlet. The outlet stop valve and vacuum pump were opened for 5–6 h.

    2. Setting confining pressure: The valve was closed at the outlet. The holder was applied with a confining pressure of 8.0 MPa.

    3. CH_4 adsorption equilibrium: The CH_4 cylinder was opened to set to a pressure of 1.5 MPa while opening the inlet valve. To ensure that the coal sample fully adsorbed the CH_4, the adsorption time was more than 24 h, and the changes in flow and pressure were monitored during the adsorption process.

    4. CO_2 injection: The CH_4 intake valve was closed, the CO_2 intake valve was opened, and the pressure was adjusted to the target value. After the pressure was balanced at both ends, the back pressure valve was adjusted, and the flow of the discharged gas was monitored and collected.

    5. Gas analysis: The outlet mixed gas was analyzed by gas chromatography.

    6. Pressure relief: The intake valve was closed. The internal pressure of the gripper was released by adjusting the back-pressure valve. The next set of tests were performed after the pressure was released.

With the increasing injection of CO_2 gas, CO_2 seeped from coal fractures and diffused into the coal matrix pores. Finally, CO_2 broke through the coal sample, and the concentration of CO_2 gradually increased, while the concentration of CH_4 gas began to decrease. Because the coal adsorption capacity to CO_2 was stronger than CH_4, CO_2 competed with CH_4 to adsorb on the pore surface, replaced the adsorbed CH_4 on the inner surface of the coal pore, and converted it into free CH_4. The migration and evolution process of CH_4 went through desorption–diffusion–seepage under the action of concentration and pressure gradient, then diffused and seeped from coal pores and coal fractures to the coal surface. The concentration changes of CH_4 and CO_2 are shown in Figure 2. The higher the pressure, the faster the decrease in the CH_4 concentration. When the concentration of CH_4 decreased to 5%, the injection pressures of 6.0 MPa, 4.0 MPa, and 2.0 MPa corresponded to the corresponding times of CH_4 change 3.8 h, 4.5 h, 5.1 h, respectively. Injection pressure also had a positive effect on the CO_2 concentration. When the concentration of CO_2 was increased to 95%, the corresponding times of CO_2 change were 3.5 h, 4.5 h, and 5.5 h at pressures of 6.0 MPa, 4.0 MPa, and 2.0 MPa, respectively. The cumulative injection amount of CO_2 was larger at higher pressures. A greater seepage force was provided by a higher injection pressure. Higher pressure provided a driving force for CH_4 migration in the coal sample and improved the sweep efficiency.
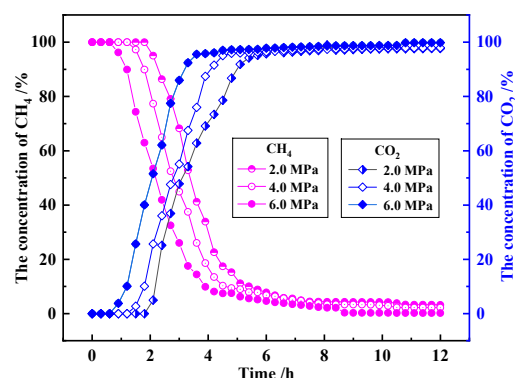

Figure 2. The CH_4 and CO_2 concentration changes under different pressures.

According to the experimental results in Table 2, the CH_4 production rates of coal samples under different pressures (2.0 MPa, 4.0 MPa, and 6.0 MPa) were 43.6%, 54.3%, and 70.7%, respectively. The CH_4 production rate is expressed as the output volume/injection volume. With the increase in pressure, the CH_4 production rate increased by 24.4% and

61.9%, respectively. The displacement ratios (CO_2 storage volume/CH_4 production volume) of CH_4 in the coal samples injected at different pressures were 3.85, 3.15, and 2.45, respectively. As the pressure increased, the displacement ratios decreased by 18.2% and 36.4%, respectively, and the sweep efficiency promoted by 12.5% and 62.2%, respectively.

Table 2. The experimental results of displacement of CH_4 by CO_2.

Order Number	Injection Volume/mL		Injection Pressure/MPa	Output Volume/mL		CO_2 Storage/mL	Replacement Ratio	Sweep Efficiency/%
	CH$_4$	CO$_2$		CH$_4$	CO$_2$			
1	779	4370	2.0	340	3060	1310	3.85	43.6
2	851	5192	4.0	462	3738	1454	3.15	54.3
3	900	6220	6.0	636	4664	1556	2.45	70.7

Figure 3 shows the change in the cumulative displacement of CH_4 under different pressure conditions. In the early stage, cumulative growth showed a linear trend. Then, it slowly rose. The cumulative displacement increased with an increase in displacement pressure. The CO_2 diffused from the pore fractures to the micropores and competed with CH_4. The diffusion velocity was much smaller than the seepage velocity. A large amount of CO_2 was discharged from the coal before it entered the pores. As a result, the storage and output rates tended to flatten. Therefore, the adsorption and storage of CO_2 in the coal seam was faster and more effective in the early stages of displacement. The sweep effect tends to be stable, while the CH_4 production rate becomes small in later stages.
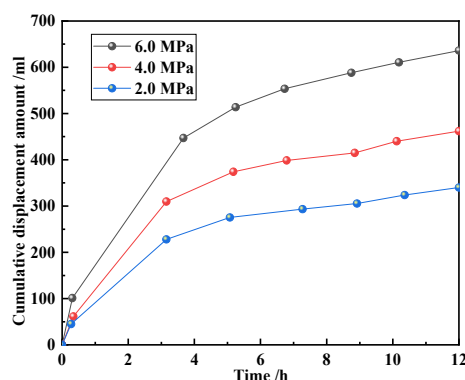

Figure 3. The curve of CH_4 cumulative displacement.

In the initial stage, the cumulative displacement of CH_4 increased rapidly and exhibited a linear growth trend. After reaching the critical time, the CH_4 desorption rate was smaller than the CO_2 displacement volume and then reached a constant value. Therefore, the cumulative amount of CH_4 displacement in the coal during the same period also changed slowly. At the beginning of the experiment, there was more free CH_4, which quickly flowed out of the coal under the displacement pressure. It can be seen that the initial CH_4 sweep efficiency is higher. After the critical time, the sweep efficiency gradually reached a constant value, and the concentration was stable at approximately 2.0%. With an increase in the displacement time, the adsorbed CH_4 in coal accounted for the majority, and there was very little free CH_4. The gas desorption rate tended to be constant, and the sweep efficiency did not change significantly.

2.3. In Situ Experiment

2.3.1. Experimental Design and System Process

This field industrial test was conducted in the return airway of the 401,101 working face in the Mengcun coal mine of Binchang mining area in Shaanxi Province. The #4 coal seam is a low metamorphic bituminous coal deposit with an average thickness of 13.0 m and an average dip angle of 3°, and it is a typical coal seam with high gas and low permeability.

The predicted value of absolute gas emission in the mine is 110.5 m^3/min, while the predicted value of relative gas emission is 8.1 m^3/t. When gas extraction is carried out by dense drilling, problems such as high cost, long extraction time, and poor extraction effect must be overcome. To solve these problems, L-CO$_2$ displacing coal seam CH$_4$ technology was used to improve the efficiency of gas drainage and provide strong support for gas disaster prevention and mine safety production.

Two groups of injection holes and a group of contrast holes were designed in the L-CO$_2$ injection test; each group designed a L-CO$_2$ injection hole and six inspection holes. There were five contrast holes in the original area. The drilling design schematic is shown in Figure 4, and the drilling design parameters are listed in Table 3.
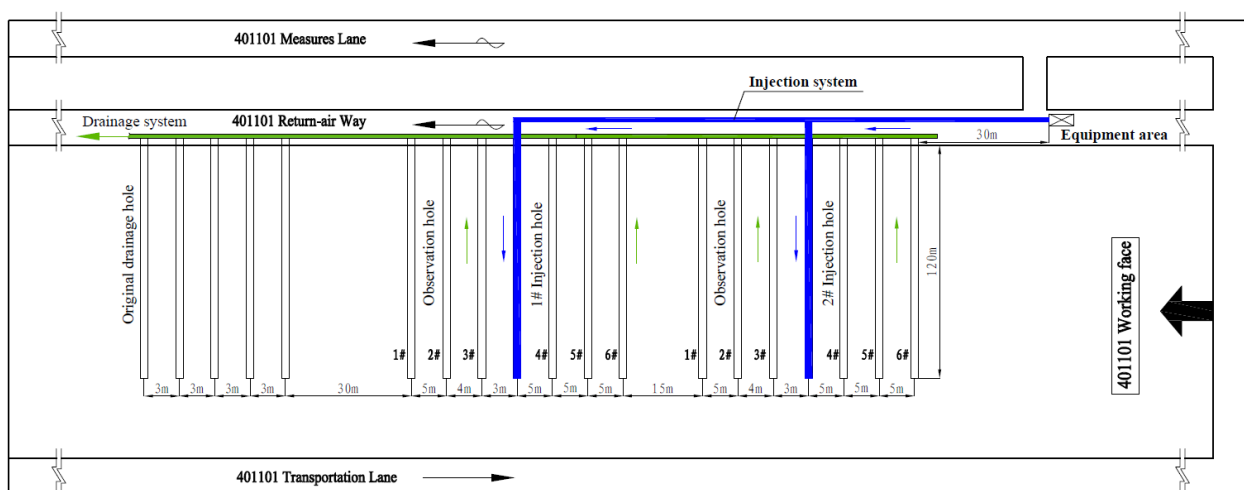

Figure 4. Schematic diagram of test borehole layout.

Table 3. Drilling design parameter table of L-CO$_2$ injection system.

Boreholes	Depth (m)	Orientation (°)	Dip Angle (°)	Aperture (mm)	Sealing Length (m)
YZ	120	90	0.5–1	133	50
K1–K6	120	90	0.5–1	133	30
D1–D5	120	90	0–0.5	133	12

A process diagram of the L-CO$_2$ injection system is shown in Figure 5. It is composed of an L-CO$_2$ injection system, data acquisition system, gas drainage system, and borehole design. The L-CO$_2$ injection system consists of an L-CO$_2$ tanker, a low-temperature booster pump (with a maximum flow rate of 2000 L/h and maximum working pressure of 15.0 MPa), pressure-resistant transmission pipeline, stop valves, and relief valves. The data acquisition system includes pressure acquisition, flow acquisition, and drainage system monitoring (drainage flow, CO$_2$ concentration, and CH$_4$ concentration). The gas extraction system includes a gas extraction pump and extraction pipeline [40,41]. When the booster pump was used, the pipeline of the injection system was pre-cooled, and the temperature condition of the pump start was set to ≤−15 °C. In order to ensure that CO$_2$ was kept in the liquid state during the injection process, the pressure of the booster pump was never less than 3.0 MPa.

The success or failure of the experiment was determined based on the sealing quality of the borehole. The length of sealing in L-CO$_2$ displacing CH$_4$ experimental drilling involves several factors such as the pressure of the sealing section, the distance of the gas discharge belt from the coal wall, and the influence of air leakage from the hole. The sealing length was determined by combining data from the actual sealing experience on site with safety factors [42,43], which ensured the safety and reliability of the experiment. The sealing lengths of the injection hole, comparison hole, and original hole were 50 m,

30 m, and 12 m, respectively. A schematic diagram of the borehole sealing is shown in Figure 6.
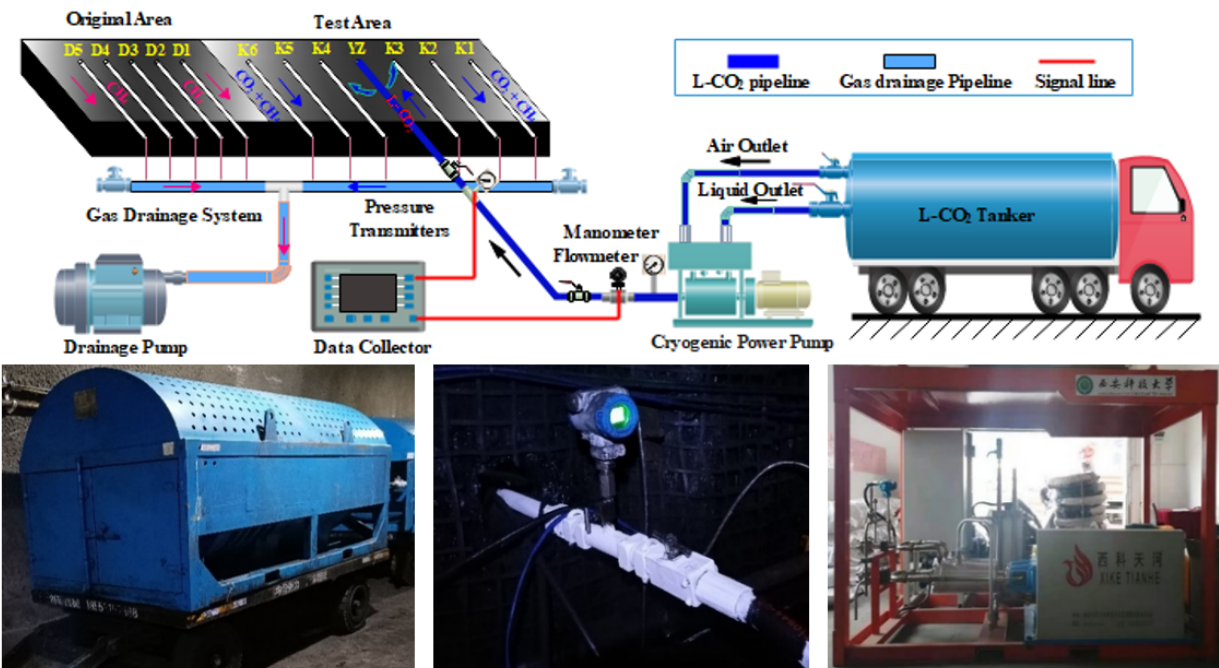

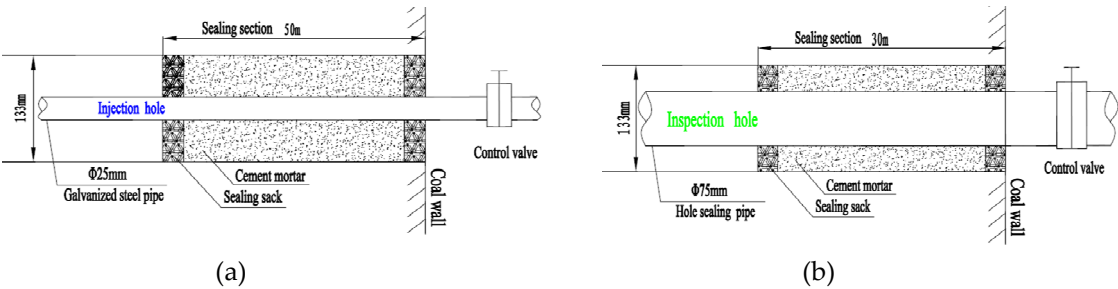**Figure 5.** Process diagram of L-CO$_2$ injection system.

Figure 6. The sealing lengths of injection hole and inspection hole (**a**) The sealing length of injection hole and (**b**) The sealing length of inspection hole.

2.3.2. Experimental Analysis

(1)　Pressure changes

The L-CO$_2$ injection tests were divided into two groups, low pressure and medium pressure. The low-pressure injection used L-CO$_2$ storage tanks to inject directly, while the medium-pressure injection utilized the L-CO$_2$ storage tank and booster pump. During the test, changes in the orifice pressure and extraction effect under different pressures were observed. The main technical indicators are listed in Table 4, and the pressure trends during the injection process are shown in Figure 7.

Table 4. Main technical indicators of L-CO$_2$ injection.

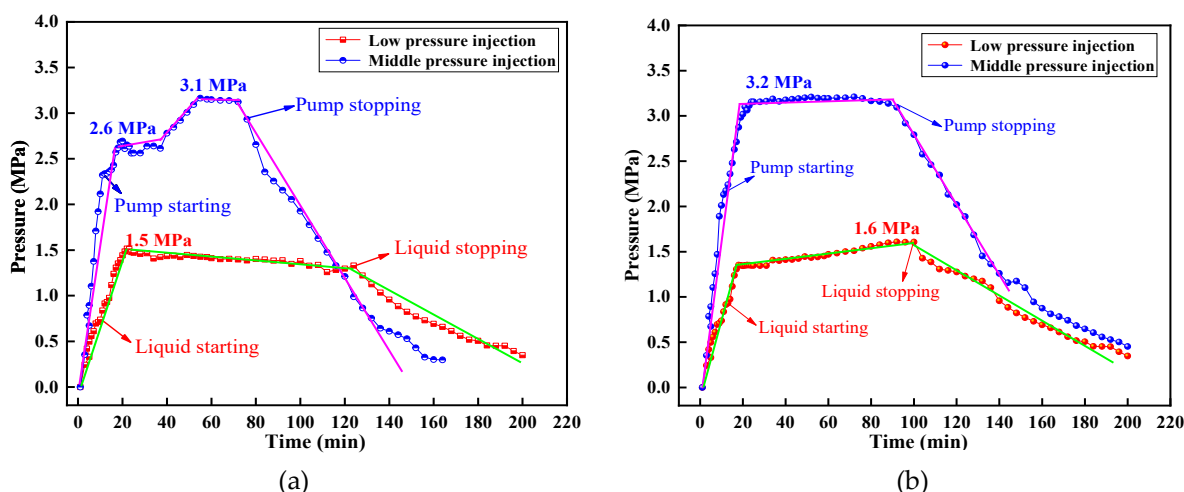| Serial Number	Boost Time of Pressure/min	Pressure Fluctuation Range/MPa	Pressure Fluctuation time/min	Maximum Pressure/MPa	Cumulative Injection Volume/m^3
1	23	1.3–1.6	110	1.52	5.9
2	17	2.5–3.2	60	3.16	5.8

Figure 7. The pressure change trend during injection (**a**) The first injection process and (**b**) The second injection process.

The diagram shows that a tank injection with a maximum pressure of 2.50 MPa was used, and the pressure was maintained for approximately 90–110 min. When the system was cooled by gas injection for a certain time, liquid CO_2 was injected, and it reached its maximum value. With continuous injection, the pressure fluctuated around 1.5–1.6 MPa and decreased slowly. L-CO_2 was supercharged by a booster pump during medium pressure injection. Figure 7a shows that the pressure reached 2.60 MPa after 17 min, and the pressure continued rising after approximately 40 min. It reached a maximum value of 3.2 MPa and fluctuated around 3.0 MPa. The fluctuation time was approximately 25 min, after which the pressure decreased rapidly. Figure 7b shows that the pressure reached a maximum value of 3.20 MPa rapidly, fluctuated around 3.2 MPa for approximately 71 min, and then decreased when the pump stopped.

The pressure increase rate of the low-pressure injection was approximately 0.066–0.075 MPa/min, and that of the medium pressure injection was approximately 0.135–0.186 MPa/min. The pressure reduction rate during the low-pressure injection was approximately 0.013 MPa/min, and that of the medium-pressure injection was approximately 0.025–0.031 MPa/min. The increase rate and reduction rate of the medium-pressure injection were larger than those of the low-pressure injection. The effective injection time was approximately 100 min when the tank was used, while the effective injection time of the tank and booster pump was approximately 65 min. When the booster pump was used for injection, the effective injection time was reduced by 35 min. The increased displacement pressure improved the time efficiency, and the increase in pressure was beneficial to gas diffusion.

(2) Analysis of displacement process

The relationship between the concentrations of CH_4 and CO_2 is shown in Figure 8. During the injection process, the change trend of the CH_4 concentration is consistent with that of the CO_2 concentration. The entire process can be divided into two stages: seepage and diffusion. The pressure gradient generated during the L-CO_2 injection and phase transition in seepage stage. The free CH_4 was driven out along the fractured channel. The initial concentration was high but decreased rapidly. At the same time, the displacement effect on the free gas was obvious, and the gas concentration was high in the initial stage. The diffusion stage occurred after the vaporization of L-CO_2 in the hole, and the concentration difference was generated by the gas. Adsorption CH_4 was replaced by CO_2 during diffusion. At that time, the gas diffused into the pores of the coal matrix through the concentration difference, and the displacement and desorption of the free CH_4 in the coal matrix and the adsorbed CH_4 were carried out. With the diffusion of CO_2, the displacement effect on a certain range of coal was gradually reduced, and the gas concentration also

declined. When the concentration of CO_2 was approximately the same as that of the original area, this stage has ended. The CO_2 in the coal seam still played a role in displacement, and the gas remained at a higher concentration relative to the original area.
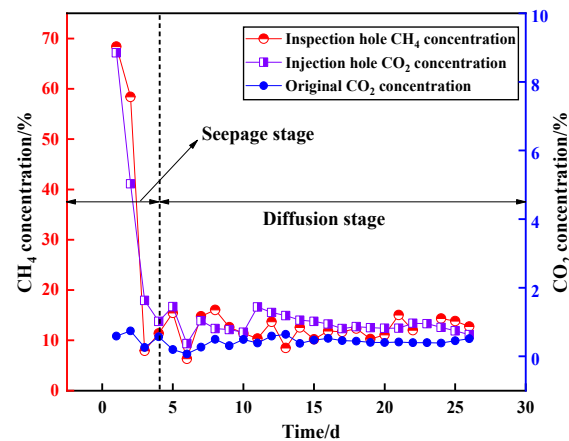

Figure 8. Relationship between CH_4 concentration and CO_2 concentration change.

(3) Seepage diffusion range for CO_2

The temperatures 3 m and 5 m from injection hole were measured by an infrared thermal imager under the medium pressure injection. The temperature decreased slowly as the distance from injection hole increased. As shown in Figure 9, when the pressure was between 2.5 MPa and 3.0 MPa, the CO_2 3 m away from the injection hole was in the liquid phase, while that 5 m away was at the critical point of liquid–gas phase. It was concluded that the L-CO_2 phase transition range and seepage range is less than 5 m.
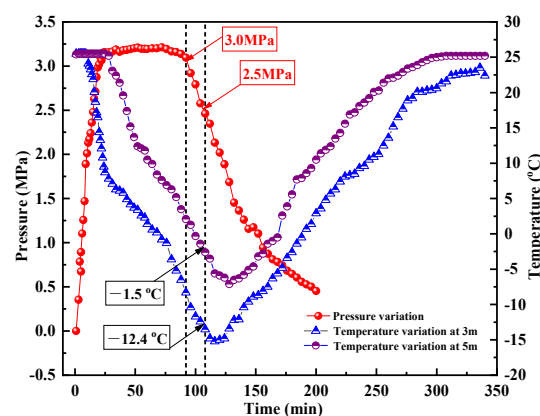

Figure 9. Temperature–pressure variation curves.

As shown in Figure 10, the CO_2 concentration changes in the inspection holes under low- and medium-pressure injections were investigated at different distances. The curve fitting formula for the CO_2 concentration change can be expressed as $y = y_0 + A \cdot e^{R_0 \cdot t}$. The fitting parameters are listed in Tables 5 and 6. At low-pressure injection, the R^2 values of Figure 10a at 5 m and 10 m from the injection hole were 0.9679 and 0.9742, respectively. The polynomial was used to fit 15 m to 30 m fitting curve, and the R^2 values of 15 m to 30 m were 0.9946, 0.9503, 0.9971 and 0.9970, respectively. After 15 m to 30 m, due to the uneven distribution of coal seam porosity and permeability, the pressure gradient of CO_2 during low-pressure injection is small; the concentration difference is small at the initial stage of diffusion, and the diffusion rate of CO_2 seepage is slow. With the passage of diffusion time and the increase in the concentration difference, the CO_2 concentration detected from 15 m

to 30 m has an increasing trend compared with the initial stage, and gradually decreased with the decrease in concentration difference in the later stage.
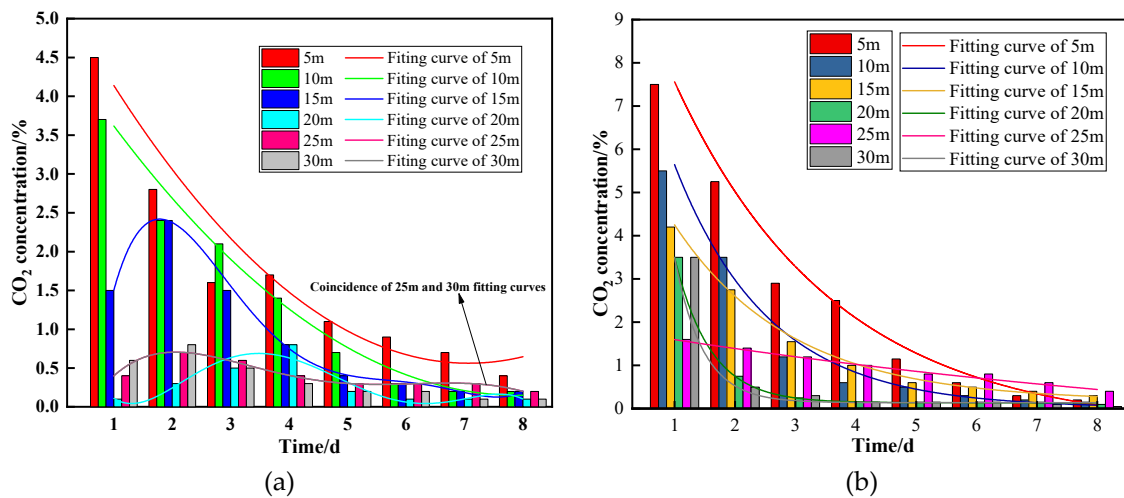

Figure 10. The change in CO_2 concentration in inspection hole (**a**) The change of CO_2 concentration during low-pressure injection and (**b**) The change of CO_2 concentration during medium-pressure injection.

Table 5. The fitting parameters of CO_2 concentration during low-pressure injection.

	y_0	A	B	R^2	Distance/m
y_1	0.51	6.56	−0.51	0.9679	5
y_2	−0.53	5.55	−0.28	0.9742	10

Table 6. The fitting parameters of CO_2 concentration during medium-pressure injection.

	y_0	A	B	R^2	Distance/m
y_1	−0.49	11.75	−0.38	0.9879	5
y_2	0.02	10.69	−0.64	0.9737	10
y_3	0.17	6.85	−0.52	0.9958	15
y_4	0.14	18.40	−1.70	0.9997	20
y_5	−1.15	2.97	−0.08	0.9818	25
y_6	0.14	28.92	−2.15	0.9965	30

For the ranges of 15 m, 20 m, 25 m, and 30 m from the injection hole, the concentration of CO_2 first increased and then decreased. Because the pressure gradient between the injection hole and the investigation hole was relatively small under low-pressure injection, the CO_2 seepage tended to be slow. With an increase in the total injection volume, the diffusion range and amount of CO_2 gradually increased under the effect of the CO_2 concentration gradient. In the medium-pressure injection, the variation trend of CO_2 concentration in each inspection hole in Figure 10b was in line with the exponential decreasing trend. The 25 m distance curve is slightly different from the other curves. The difference in the permeability and inhomogeneity of coal fracture development on both sides of the injection hole affected the seepage diffusion of CO_2. Under the medium-pressure injection, the CO_2 seepage diffusion velocity and concentration were higher. The original contrast-hole CO_2 concentration was 0.43%. The diffusion range of CO_2 under low-pressure injection was 20–25 m, while under medium pressure injection it was 25–30 m. Therefore, a higher displacement pressure can effectively promote the displacement of CH_4 by L-CO_2.

(4)   Analysis of the displacement effect

The average gas drainage concentration and drainage purity during low-pressure and medium-pressure injections are presented in Figures 11 and 12, respectively. The average gas extraction concentration in the original area was 3.23%, and the average gas extraction purity was 0.00028 m^3/min. The average gas drainage concentration of the monitoring borehole during low-pressure injection was 5.19%, and the average gas drainage purity was 0.00059 m^3/min. The average gas extraction concentration during low-pressure injection was 1.61 times that of the original area, and the average gas extraction purity was 2.08 times that of the original area. The average gas extraction concentration of the monitoring borehole during medium-pressure injection was 7.02%, and the average gas extraction purity was 0.00083 m^3/min. The average gas extraction concentration during medium-pressure injection was 2.17 times that of the original area, and the average gas extraction purity was 2.94 times that of the original area. The medium-pressure injection of average gas extraction concentration was 1.35 times of that of the low-pressure injection, and the medium-pressure injection of average gas extraction purity was 1.41 times of that of the low-pressure injection. The medium-pressure injection was more efficient.
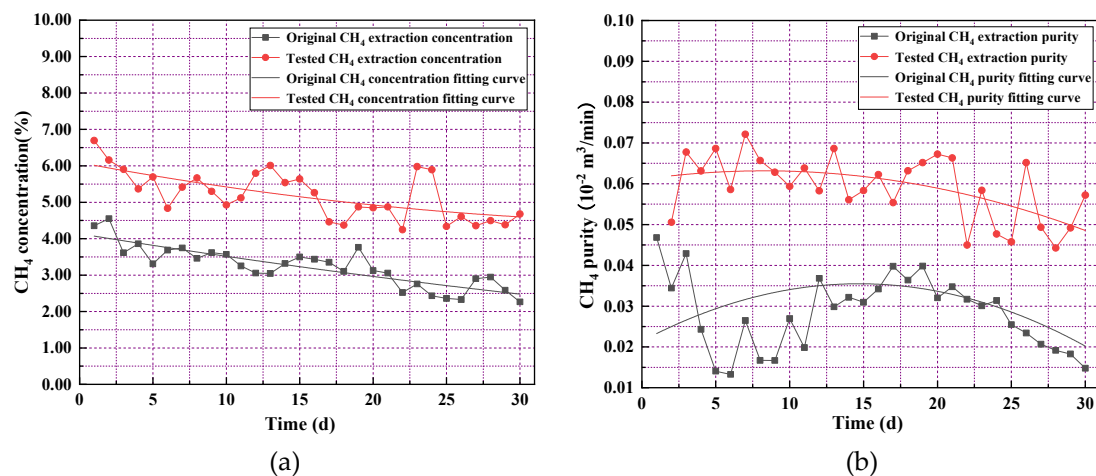

Figure 11. Average gas drainage concentration and drainage purity during low-pressure injection (**a**) Average gas drainage concentration and (**b**) Average gas drainage purity.
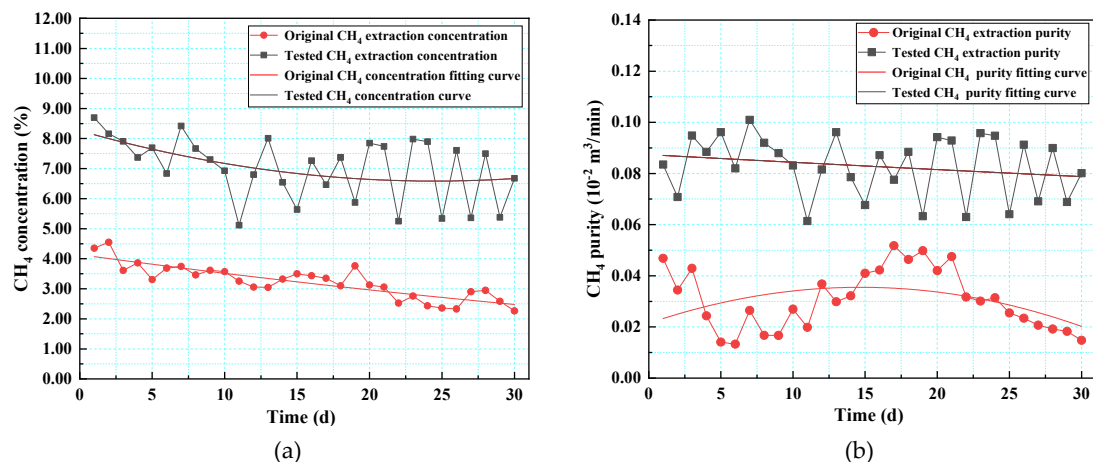

Figure 12. Average gas drainage concentration and drainage purity during medium-pressure injection (**a**) Average gas drainage concentration and (**b**) Average gas drainage purity.

(5) Comparison of sweep efficiency

In the field test, to analyze the displacement effect under different pressures, the sweep efficiency was determined by comparing the total amount of displacement gas.

$$\eta = \frac{\varphi_t \cdot \rho_t - \varphi_0 \cdot \rho_0}{\varphi_t \cdot \rho_t} \tag{5}$$

where η represents gas drainage efficiency, φ_t and ρ_t are the gas drainage flow and gas drainage concentration after displacement, respectively; φ_0 and ρ_0 are the gas drainage flow and gas drainage concentration before displacement, respectively.

The low- and medium-pressure gas drainage data can be calculated using Formula (5). The gas extraction efficiency in low-pressure injection η_L was 52.4%, while the gas extraction efficiency in medium-pressure injection η_M was 66.0%. The sweep efficiency of the medium-pressure injection (average pressure—2.8 MPa) was 26% higher than that of the low-pressure injection (average pressure—1.4 MPa).

In the displacement experiment, the variation law of CH_4 and CO_2 concentration under different pressure injection conditions was obtained, and the variation law of the concentration showed the rule of "alternating growth and decline". At the same time, the injection pressure has a positive effect in the experimental process: the higher the pressure, the higher the displacement efficiency, and the greater the cumulative displacement. Combined with the laboratory results of CO_2 displacement coal seam CH_4, in the field test of liquid CO_2 displacement coal seam CH_4 under different pressure conditions, the injection pressure also has a positive effect on the improvement of displacement efficiency, influence range and gas extraction effect. Therefore, a CO_2 displacement experiment in the laboratory provides research foundation and theoretical basis for field tests.

3. Conclusions

(1) The CH_4 production rates under different pressures (2.0 MPa, 4.0 MPa, and 6.0 MPa) were 43.6%, 54.3%, and 70.7%, respectively. With the increase in pressure, the CH_4 production rate increased by 24.4% and 61.9%, respectively. The displacement ratios of CH_4 in the coal samples injected with different pressures were 3.85, 3.15, and 2.45. As the pressure increased, the displacement ratios decreased by 18.2% and 36.4%, respectively, and the sweep efficiency increased by 12.5% and 62.2%, respectively. Increasing the pressure improved the CH_4 sweep efficiency and decreased the displacement ratio.

(2) The maximum pressure of the low-pressure injection was 1.52 MPa, while the maximum pressure of the medium-pressure injection was 3.16 MPa. The pressure was 2.1 times that of the low-pressure injection. The pressure rise rate was 2.82 times that of low-pressure injection, and the pressure drop rate was 1.32 times that of the low-pressure injection. (3) Through a comparative analysis of the change trend of the CH_4 concentration and CO_2 concentration in the observation hole, it was determined that the change trend remained the same. The process of L-CO_2 displacing gas can be roughly divided into two stages: the seepage stage and the diffusion stage. In the seepage stage, CO_2 had a more obvious driving effect on free gas, and the gas concentration was relatively high in the initial stage. In the diffusion stage, CO_2 played a major role in the displacement and desorption of adsorbed gas, and the gas concentration gradually decreased. A higher displacement pressure effectively promoted the displacement of CH_4 by L-CO_2. The diffusion range of CO_2 under the low-pressure injection was 20–25 m, while under medium-pressure injection it was 25–30 m.

(3) Inspection of the gas extraction field revealed that the concentration of CH_4 extracted increased from 3.23% to 5.19% after the low-pressure injection of L-CO_2 into the coal seam, increasing the concentration of gas extracted by 0.61 times. The pure flow of gas extracted increased from 0.028 m^3/min to 0.059 m^3/min, increasing the pure flow of gas extracted by 1.08 times. The concentration of CH_4 extracted increased

from 3.23% to 7.02% after the medium-pressure injection of L-CO_2 into the coal seam, increasing the concentration of gas extracted by 1.17 times. The pure flow of gas extracted increased from 0.028 m^3/min to 0.083 m^3/min, increasing the pure flow of gas extracted by 1.94 times. The average gas drainage concentration of the medium-pressure injection was 1.35 times that of the low-pressure injection, and the average gas drainage scalar medium-pressure injection was 1.41 times that of low-pressure injection. The sweep efficiency of the medium-pressure injection (average pressure—2.8 MPa) was 26% higher than that of the low-pressure injection (average pressure—1.4 MPa). The overall efficiency of the medium-pressure injection was much higher.

Through this test, the displacement technology of coal seam CH_4 by injection of L-CO_2 proved to significantly improve gas drainage efficiency. An increase in pressure is beneficial for improving the sweep efficiency of L-CO_2. This field test only carried out displacement tests under two pressure conditions, and the experimental results have important significance for field gas drainage. Due to the influence of various mine production factors, it is impossible to carry out more displacement tests under pressure conditions and different flow conditions. As the test is difficult to implement in the field, it is still necessary to study displacement field tests under different pressure and different flow conditions in the future.

References

1. Zhou, F.; Xia, T.; Wang, X.; Zhang, Y.; Sun, Y.; Liu, J. Recent developments in coal mine methane extraction and utilization in China: A review. *J. Nat. Gas Sci. Eng.* **2016**, *31*, 437–458. [CrossRef]
2. Zhang, D.; Cen, X.; Wang, W.; Deng, J.; Wen, H.; Xiao, Y.; Shu, C.-M. The graded warning method of coal spontaneous combustion in Tangjiahui Mine. *Fuel* **2021**, *288*, 119635. [CrossRef]
3. Chen, X.; Li, L.; Wang, L.; Qi, L. The current situation and prevention and control countermeasures for typical dynamic disasters in kilometer-deep mines in China. *Saf. Sci.* **2019**, *115*, 229–236. [CrossRef]
4. Wei, G.; Wen, H.; Deng, J.; Ma, L.; Li, Z.; Lei, C.; Fan, S.; Liu, Y. Liquid CO_2 injection to enhance coalbed methane recovery: An experiment and in-situ application test. *Fuel* **2021**, *284*, 119043. [CrossRef]
5. Li, Z.; Wei, G.; Liang, R.; Shi, P.; Wen, H.; Zhou, W. LCO_2-ECBM technology for preventing coal and gas outburst: Integrated effect of permeability improvement and gas displacement. *Fuel* **2021**, *285*, 119219. [CrossRef]
6. Lin, J.; Ren, T.; Cheng, Y.; Nemcik, J.; Wang, G. Cyclic N2 injection for enhanced coal seam gas recovery: A laboratory study. *Energy* **2019**, *188*, 116115. [CrossRef]
7. Durucan, S.; Shi, J.-Q. Improving the CO_2 well injectivity and enhanced coalbed methane production performance in coal seams. *Int. J. Coal Geol.* **2009**, *77*, 214–221. [CrossRef]
8. Wen, H.; Li, Z.; Deng, J.; Shu, C.-M.; Laiwang, B.; Wang, Q.; Ma, L. Influence on coal pore structure during liquid CO_2-ECBM process for CO_2 utilization. *J. CO_2 Util.* **2017**, *21*, 543–552. [CrossRef]
9. Qin, L.; Li, S.; Zhai, C.; Lin, H.; Zhao, P.; Shi, Y.; Bai, Y. Changes in the pore structure of lignite after repeated cycles of liquid nitrogen freezing as determined by nitrogen adsorption and mercury intrusion. *Fuel* **2020**, *267*, 117214. [CrossRef]
10. Wen, H.; Cheng, X.; Chen, J.; Zhang, C.; Yu, Z.; Li, Z.; Fan, S.; Wei, G.; Cheng, B. Micro-pilot test for optimized pre-extraction boreholes and enhanced coalbed methane recovery by injection of liquid carbon dioxide in the Sangshuping coal mine. *Process Saf. Environ. Prot.* **2020**, *136*, 39–48. [CrossRef]

11. Yan, F.; Lin, B.; Zhu, C.; Shen, C.; Zou, Q.; Guo, C.; Liu, T. A novel ECBM extraction technology based on the integration of hydraulic slotting and hydraulic fracturing. *J. Nat. Gas Sci. Eng.* **2015**, *22*, 571–579. [CrossRef]

12. Ranathunga, A.S.; Perera, M.S.A.; Ranjith, P.G.; Zhang, X.G.; Wu, B. Super-critical carbon dioxide flow behaviour in low rank coal: A meso-scale experimental study. *J. CO₂ Util.* **2017**, *20*, 1–13. [CrossRef]

13. Sander, R.; Pan, Z.; Connell, L.D. Laboratory measurement of low permeability unconventional gas reservoir rocks: A review of experimental methods. *J. Nat. Gas Sci. Eng.* **2017**, *37*, 248–279. [CrossRef]

14. Zou, Q.; Lin, B. Fluid–Solid Coupling Characteristics of Gas-Bearing Coal Subjected to Hydraulic Slotting: An Experimental Investigation. *Energy Fuels* **2018**, *32*, 1047–1060. [CrossRef]

15. Busch, A.; Gensterblum, Y. CBM and CO_2-ECBM related sorption processes in coal: A review. *Int. J. Coal Geol.* **2011**, *87*, 49–71. [CrossRef]

16. Zhou, F.; Hussain, F.; Cinar, Y. Injecting pure N_2 and CO_2 to coal for enhanced coalbed methane: Experimental observations and numerical simulation. *Int. J. Coal Geol.* **2013**, *116–117*, 53–62. [CrossRef]

17. Vishal, V. In-situ disposal of CO_2: Liquid and supercritical CO_2 permeability in coal at multiple down-hole stress conditions. *J. CO₂ Util.* **2017**, *17*, 235–242. [CrossRef]

18. Lin, J.; Ren, T.; Wang, G.; Booth, P.; Nemcik, J. Experimental investigation of N_2 injection to enhance gas drainage in CO_2-rich low permeable seam. *Fuel* **2018**, *215*, 665–674. [CrossRef]

19. Syah, R.; Alizadeh, S.M.; Darvishzadeh, L.; Elveny, M.; Abedi, M.; Ramdan, D. Simultaneous injection of chemical agents and carbon dioxide to enhance the sweep efficiency from fractured tight core samples. *Energy Rep.* **2021**, *7*, 5639–5646. [CrossRef]

20. Kumar, H.; Elsworth, D.; Mathews, J.P.; Liu, J.; Pone, D. Effect of CO_2 injection on heterogeneously permeable coalbed reservoirs. *Fuel* **2014**, *135*, 509–521. [CrossRef]

21. Merkel, A.; Gensterblum, Y.; Krooss, B.M.; Amann, A. Competitive sorption of CH_4, CO_2 and H_2O on natural coals of different rank. *Int. J. Coal Geol.* **2015**, *150–151*, 181–192. [CrossRef]

22. Dutka, B.; Kudasik, M.; Pokryszka, Z.; Skoczylas, N.; Topolnicki, J.; Wierzbicki, M. Balance of CO_2/CH_4 exchange sorption in a coal briquette. *Fuel Process. Technol.* **2013**, *106*, 95–101. [CrossRef]

23. Liu, Z.; Cheng, Y.; Wang, Y.; Wang, L.; Li, W. Experimental investigation of CO_2 injection into coal seam reservoir at in-situ stress conditions for enhanced coalbed methane recovery. *Fuel* **2019**, *236*, 709–716. [CrossRef]

24. Kumar, H.; Elsworth, D.; Liu, J.; Pone, D.; Mathews, J.P. Optimizing enhanced coalbed methane recovery for unhindered production and CO_2 injectivity. *Int. J. Greenh. Gas Control* **2012**, *11*, 86–97. [CrossRef]

25. Kim, S.; Ko, D.; Mun, J.; Kim, T.-H.; Kim, J. Techno-economic evaluation of gas separation processes for long-term operation of CO_2 injected enhanced coalbed methane (ECBM). *Korean J. Chem. Eng.* **2018**, *35*, 941–955. [CrossRef]

26. Topolnicki, J.; Kudasik, M.; Dutka, B. Simplified model of the CO_2/CH_4 exchange sorption process. *Fuel Process. Technol.* **2013**, *113*, 67–74. [CrossRef]

27. Mazzotti, M.; Pini, R.; Storti, G. Enhanced coalbed methane recovery. *J. Supercrit. Fluids* **2009**, *47*, 619–627. [CrossRef]

28. Bai, X.; Zhang, D.; Zeng, S.; Zhang, S.; Wang, D.; Wang, F. An enhanced coalbed methane recovery technique based on CO_2 phase transition jet coal-breaking behavior. *Fuel* **2020**, *265*, 116912. [CrossRef]

29. Wang, J.; Liu, J.; Li, Z.; Li, H.; Zhang, J.; Li, W.; Zhang, Y.; Ping, Y.; Yang, H.; Wang, P. Synchronous injection-production energy replenishment for a horizontal well in an ultra-low permeability sandstone reservoir: A case study of Changqing oilfield in Ordos Basin, NW China. *Pet. Explor. Dev.* **2020**, *47*, 827–835. [CrossRef]

30. Chen, H.; Wang, Z.; Chen, X.; Chen, X.; Wang, L. Increasing permeability of coal seams using the phase energy of liquid carbon dioxide. *J. CO₂ Util.* **2017**, *19*, 112–119. [CrossRef]

31. Wei, G.; Wen, H.; Deng, J.; Li, Z.; Fan, S.; Lei, C.; Liu, M.; Ren, L. Enhanced coalbed permeability and methane recovery via hydraulic slotting combined with liquid CO_2 injection. *Process Saf. Environ. Prot.* **2021**, *147*, 234–244. [CrossRef]

32. Vishal, V. Saturation time dependency of liquid and supercritical CO_2 permeability of bituminous coals: Implications for carbon storage. *Fuel* **2017**, *192*, 201–207. [CrossRef]

33. Wen, H.; Wei, G.; Ma, L.; Li, Z.; Lei, C.; Hao, J. Damage characteristics of coal microstructure with liquid CO_2 freezing-thawing. *Fuel* **2019**, *249*, 169–177. [CrossRef]

34. Fujioka, M.; Yamaguchi, S.; Nako, M. CO_2-ECBM field tests in the Ishikari Coal Basin of Japan. *Int. J. Coal Geol.* **2010**, *82*, 287–298. [CrossRef]

35. Liang, W.; Zhao, Y.; Wu, D.; Dusseault, M.B. Experiments on Methane Displacement by Carbon Dioxide in Large Coal Specimens. *Rock Mech. Rock Eng.* **2011**, *44*, 579–589. [CrossRef]

36. Perera, M.S.A.; Ranjith, P.G.; Airey, D.W.; Choi, S.K. Sub- and super-critical carbon dioxide flow behavior in naturally fractured black coal: An experimental study. *Fuel* **2011**, *90*, 3390–3397. [CrossRef]

37. Godec, M.; Koperna, G.; Gale, J. CO_2-ECBM: A Review of its Status and Global Potential. *Energy Procedia* **2014**, *63*, 5858–5869. [CrossRef]

38. Zhang, X.; Ranjith, P.G. Experimental investigation of effects of CO_2 injection on enhanced methane recovery in coal seam reservoirs. *J. CO₂ Util.* **2019**, *33*, 394–404. [CrossRef]

39. Al-Abri, A.; Sidiq, H.; Amin, R. Mobility ratio, relative permeability and sweep efficiency of supercritical CO_2 and methane injection to enhance natural gas and condensate recovery: Coreflooding experimentation. *J. Nat. Gas Sci. Eng.* **2012**, *9*, 166–171. [CrossRef]

40. Wen, H.; Liu, M.; Wei, G.; Zhai, X.; Fan, S.; Cheng, X.; Wang, H.; Hao, J.; Xia, B.-W. Gas Displacement Engineering Test by Combination of Low and Medium Pressure Injection with Liquid CO_2 in High Gas and Low Permeability Coal Seam. *Geofluids* **2020**, *2020*, 8840602. [CrossRef]

41. Wen, H.; Wang, H.; Fan, S.; Li, Z.; Chen, J.; Cheng, X.; Cheng, B.; Yu, Z. Improving coal seam permeability and displacing methane by injecting liquid CO_2: An experimental study. *Fuel* **2020**, *281*, 118747. [CrossRef]

42. Fan, S.; Zhang, D.; Wen, H.; Cheng, X.; Liu, X.; Yu, Z.; Hu, B. Enhancing coalbed methane recovery with liquid CO_2 fracturing in underground coal mine: From experiment to field application. *Fuel* **2021**, *290*, 119793. [CrossRef]

43. Zhao, W.; Cheng, Y.; Pan, Z.; Wang, K.; Liu, S. Gas diffusion in coal particles: A review of mathematical models and their applications. *Fuel* **2019**, *252*, 77–100. [CrossRef]